FINITE ELEMENT ANALYSIS OF CONE PENETRATION IN SOIL FOR PREDICTION OF HARDPAN LOCATION

M. Z. Tekeste, R. L. Raper, E. W. Tollner, T. R. Way

ABSTRACT. *An accurate determination of soil hardpan location is important for maximum precision tillage performance. Cone penetrometers are often used to locate hardpans in soils. This determination in layered soils is more complex due to the complexity of soil reaction to cone penetration. An axisymmetric finite element (FE) model was developed to simulate cone penetration for the prediction of the hardpan location in a layered Norfolk sandy loam soil. The soil was considered as a non-linear elastic-plastic material, and it was modeled using a Drucker-Prager model with the Hardening option in ABAQUS, a commercially available FE package. ABAQUS/Explicit was used to simulate soil-cone contact pair interaction. The results showed that the FE model captured the penetration resistance trend with two deflection points indicating the start of the hardpan and the peak cone penetration resistance. The FE-predicted results showed the hardpan at a depth of 7.29 cm compared to 11.08 cm from cone penetration tests. Soil moisture, bulk density, and cone surface conditions significantly affected the predicted and experimental results. The simulation also showed soil deformation zones about 3 times the diameter of the cone that developed around the advancing cone.*

Keywords. Adaptive meshing, Cone penetrometer, Finite element, Soil-cone interaction, Soil hardpan.

S oils in the southeastern U.S. develop highly compacted sub-surface layers, commonly referred to as hardpans, that impede root growth, which consequently affects crop production (Raper et al., 2005). Soil compaction can be measured using a soil-cone penetrometer, an instrument that measures resistance to penetration of a cone into the soil (*ASAE Standards*, 1999a, 1999b). As a part of site-specific soil compaction management, the cone penetrometer data are often used to determine the hardpan location. The reaction of the soil to cone penetration involves cutting, compression, shear or plastic failures, or any combination of these (Gill and VandenBerg, 1968). As the cone advances into the soil, the penetration resistance gives an indication of the relative strength of the soil it is encountering. Researchers have shown that the cone penetration resistance is influenced by the soil properties in the zone of influence (Gill, 1968; Sanglerat, 1972; Mulqueen et al., 1977; Lunne et al., 1997; Susila and Hryciw, 2003). According to Lunne et al. (1997), the zone of influence depends on layering and soil material stiffness, and it can reach up to

10 to 20 times the cone diameter for stiff soil material. Mulqueen et al. (1977) and Gill (1968) also showed that a soil wedge forming in front of the cone could erroneously increase the cone penetration reading.

Due to complex interactions of the soil and cone penetrometer, errors can occur in interpreting cone penetration resistance-depth data, which can affect the accuracy of hardpan detection for precision tillage. In predicting hardpan location, a study of the dynamic response of the soil to cone penetration is important. Various approaches (Farrell and Greacen, 1966; Rohani and Baladi, 1981; Tollner et al., 1987; Yu and Mitchel, 1998) have been used to study the mechanical responses of soils during cone penetration. Yu and Mitchel (1998) reviewed the analysis of cone penetration resistance using the approaches of bearing capacity theory, cavity expansion theory, steady-state deformation, finite element (FE) analysis, and laboratory experimental methods. In their study to simulate the penetration resistance of plant roots, Farrell and Greacen (1966) used cavity expansion theory to explain the resistance to penetration of fine probes in compressible soils. Tollner et al. (1987) conducted experiments in plastic chambers to study soil responses to cone penetration from lubricated and non-lubricated cone penetrometers using X-ray computer tomography (CT). Most of these approaches used analytical methods whereby a certain shape of soil failure surface was assumed and then the limit equilibrium of forces over the soil-tool system was solved. Analytical approaches may not be ideal to explain the dynamic responses of soil during cone penetration, especially in layered and heterogeneous soils, because of the difficulty involved in pre-defining the shape of the soil failure zone and force equilibrium analysis.

With the availability of powerful computers with high computational speeds and advanced soil material constitutive models, the FE method can be implemented in solving the cone penetration problem in soils. The FE method has

The authors are **Mehari Z. Tekeste, ASABE Member Engineer,** Former Graduate Assistant, Department of Biological and Agricultural Engineering, University of Georgia, Athens, Georgia; **Randy L. Raper, ASABE Member Engineer,** Agricultural Engineer, USDA-ARS National Soil Dynamics Laboratory, Auburn, Alabama; **Ernest W. Tollner, ASABE Member Engineer,** Professor, Department of Biological and Agricultural Engineering, University of Georgia, Driftmier Engineering Center, Athens, Georgia; and **Thomas R. Way, ASABE Member Engineer,** Agricultural Engineer, USDA-ARS National Soil Dynamics Laboratory, Auburn, Alabama. **Corresponding author:** Mehari Z. Tekeste, Department of Agriculture, Western Kentucky University, Bowling Green, KY 42101; phone: 270-745-5968; fax: 270-745-5972; e-mail: mehari.tekeste@ wku.edu.

been used to model cone penetration in soils with limited success (Markauskas et al., 2002; Foster et al., 2005). Markauskas et al. (2002) used static elastic-plastic small strain FE analysis on sandy and clayey soils with Mohr-Coulomb and Tresca yield criteria, respectively. They simulated the penetration of a cone (apex angle = 60° and base diameter d = 3.57 cm) to a depth (u) of 0.2d. They also predicted the vertical (H = 11.2d) and horizontal (D = 35d) dimensions of the zone influenced by the penetration. The small strain assumption, as opposed to the large strain, which is a characteristic behavior of soils under loading, was a limitation in their analysis. The authors did not experimentally verify the predicted results.

Soil cone penetration in a sandy loam and a clay loam soil was also modeled using the MSC/DYTRAN FE software by Foster et al. (2005). The constitutive material parameters used in this analysis were estimated using the National Soil Dynamics Laboratory and Auburn University (NSDL-AU) soil compaction model (Bailey and Johnson, 1989). The FE simulation study by Foster et al. (2005) was validated using cone penetration test data obtained on Norfolk sandy loam soil with initial bulk density of 1.35 Mg m^{-3} in the loose top layer and 1.68 Mg m^{-3} in the hardpan layer. Their FE simulation for Norfolk sandy loam soil had large fluctuations and increased with depth, even though the measured cone penetration resistance data showed the presence of a hardpan layer. Statistical comparisons of the predicted and experimental results were not carried out to verify the performance of the FE simulation.

Further research on FE analysis is thus needed to understand the soil deformation patterns in cone penetration and evaluate the FE method in effectively simulating the cone penetration in layered and heterogeneous soils. Therefore, our objectives were, to:

- Determine the potential use of the FE method for simulating cone penetration and predicting hardpan location in soils.
- Determine the effects of soil moisture content, bulk density, and cone surface condition on penetration resistance and hardpan location.

MATERIALS AND METHODS

MATERIAL PARAMETERS FOR SOIL CONSTITUTIVE MODEL

Soil was assumed to be a continuum non-linear elastic-plastic material that exhibited material hardening. The soil constitutive relationship was defined using the linear form of the extended Drucker-Prager material model with a material hardening option (ABAQUS, 2004). The extended Drucker-Prager model has the capability to model frictional materials, such as soil, in which compressive yield strength is greater than the tensile strength and yield is pressure dependent. The Drucker-Prager model has been used to solve soil-tool interaction problems (Mouazen and Ramon, 2002; Upadhyaya et al., 2002). The material parameters required for the FE analysis were: bulk density (ρ), Young's modulus (E), Poisson's ratio (ν), angle of friction (β), yield stress ratio in triaxial tension to triaxial compression (K), and dilation angle (ψ) for the plastic flow. The angle of friction (β) of the linear Drucker-Prager yield criterion is related to the angle of friction (φ) of the Mohr-Coulomb criterion (Chen and Mizuno, 1990) using the following equation:

$$\tan \beta = \frac{6 \sin \phi}{3 - \sin \phi} \tag{1}$$

An angle β of 38° was estimated from the linear relationship of the octahedral shear stress and octahedral normal stress states of the NSDL-AU model at yield by plastic flow, which was similar to the linear Drucker-Prager yield function with an intercept of zero (Bailey and Johnson, 1989, 1994). Associative plasticity was assumed for defining the flow rule, with the angle of dilation (ψ) assumed to be the same as the angle of friction (β). Typical values of K are $0.778 \leq K \leq 1.0$ (ABAQUS, 2004). A value of K = 1 was assumed during the analysis, implying that the yield surface was the von Mises circle in a deviatoric principal stress plane. A constant Poisson's ratio of 0.3 was assumed in the analysis. The NSDL-AU constitutive soil model (Bailey and Johnson, 1989) that was developed for compactable agricultural soils subjected to different stress paths under unsaturated soil conditions was used to estimate soil mechanical parameters and the tabular data (yield stress vs. plastic strain) for the Drucker-Prager Hardening option. The soil mechanical parameters of NSDL-AU model are shown in table 1. The estimated natural volumetric strain levels of the NSDL-AU model were modified to account for the soil moisture and bulk density values used in the experiment to verify the FE model.

According to Bailey and Johnson (1989, 1996), the stress-strain relationship of the NSDL-AU soil compaction model was defined using:

$$\bar{\varepsilon}_v = (A + B\sigma_{oct})(1 - e^{-C\sigma_{oct}}) + D(\hat{o}_{oct}/\sigma_{oct}) \tag{2}$$

where the natural volumetric strain was defined as:

$$\bar{\varepsilon}_v = \ln(V/V_o) = \ln(\rho_o/\rho) \tag{3}$$

where

$\bar{\varepsilon}_v$ = natural volumetric strain

σ_{oct} = octahedral or mean normal stress ($\sigma_{oct} = [\sigma_1 + \sigma_2 + \sigma_3] / 3$)

τ_{oct} = octahedral shear stress ($\tau_{oct} = [(\sigma_1 - \sigma_2)^2 + (\sigma_2 - \sigma_3)^2 + (\sigma_1 - \sigma_3)^2]^{1/2} / 3$)

σ_1 = major principal stress

σ_2 = intermediate principal stress

Table 1. Soil parameters and coefficients of the NSDL-AU soil compaction model for Norfolk sandy loam soil.

Soil MC (% d.b.)	Initial Bulk Density (Mg m^{-3})	Soil – Soil Angle of Internal Friction[a] (μ)	Poisson's Ratio (ν)	NSDL-AU Model Coefficients[b]				
				A	B (kPa^{-1})	C (kPa^{-1})	D	α[c]
6.3	1.35	58	0.3	−0.241	0.0002	0.0126	−0.1122	0.926

[a] Material angle of friction for Norfolk sandy loam soil from Chiroux et al. (2005).

[b] A, B, C, and D are model coefficients for the NSDL-AU soil compaction model from Bailey and Johnson (1989).

[c] α is the slope of a straight regression line fit to data in a graph of the plastic natural volumetric strain as a function of total natural volumetric strain, from Foster et al. (2005).

σ_3 = minor principal stress
V = volume at stress state
V_o = initial volume
ρ = dry bulk density at stress state
ρ_o = initial dry bulk density
A, B, C, D = compactibility coefficients for a specific soil at a specific soil moisture content.

Bailey and Johnson (1989, 1996) also found a linear relationship between the total natural volumetric strain and the natural plastic volumetric strain according to:

$$d\overline{\varepsilon}_v^p = \alpha \, d\overline{\varepsilon}_v \qquad (4)$$

where $\overline{\varepsilon}_v^p$ is the natural plastic volumetric strain, and α is a constant.

The coefficients of the NSDL-AU soil model (eq. 2) for Norfolk sandy loam soil was developed at a specific soil moisture content (6.3% d.b.). Modification of the stress-strain relationship was needed to account for different soil moisture contents and bulk density values. Johnson (personal communication, October 2004) suggested a relationship between the bulk density ratios of triaxial tests and Proctor Density curves (eq. 5). He proposed that the ratio of bulk density at one soil moisture content (e.g., 6.3% d.b.) to bulk density at a different soil moisture content of the same triaxial stress test may be related to the bulk density ratios estimated from the Proctor Density curve at the corresponding soil moisture contents.

Mathematically, the ratio of bulk density is expressed as:

$$\left[\frac{\rho_x}{\rho_i}\right]_\sigma \propto f\left\{\left[\frac{\rho_x}{\rho_i}\right]_{PD}\right\} \qquad (5)$$

where

$\left[\dfrac{\rho_x}{\rho_i}\right]_\sigma$ = dry bulk density ratio at triaxial stress state for new soil moisture content (x) relative to soil moisture content (i) of 6.3% d.b.

$\left[\dfrac{\rho_x}{\rho_i}\right]_{PD}$ = dry bulk density ratios from Proctor Density curve for new soil moisture content (x) relative to soil moisture content (i) of 6.3% d.b.

The relationship in equation 5 was evaluated using data from triaxial tests (Bailey, 2004) and from a Proctor Density curve (Grisso, 1985). A linear relationship of observed dry bulk density and predicted dry bulk density (ρ_x) for the Norfolk sandy loam soil was statistically tested using SAS (SAS, 2001).

Based on the bulk density ratio relationships, the natural volumetric strain values for different soil moisture contents were estimated using:

$$\overline{\varepsilon}_{vx} = \overline{\varepsilon}_v + \ln\left(\frac{\rho_i}{\rho_x}\right)_{PD} \qquad (6)$$

where $\overline{\varepsilon}_{vx}$ is the natural volumetric strain at new soil moisture content (x).

The hydrostatic yield stress versus volumetric plastic strain data for the Drucker-Prager Hardening option was generated from the natural volumetric stress-strain relationship (eq. 6). The relationship defined in equation 4 was used to obtain the volumetric plastic strain values. Tangential

Young's modulus values were estimated from the stress-strain graphs. The mean of the estimated tangential Young's modulus was used in the analysis. The dry bulk density and soil moisture contents for the modification of the material constitutive parameters were obtained from experiments conducted in a soil column.

FE PROBLEM FORMULATION AND PROCEDURES
ABAQUS/Explicit Solutions for Quasi-Static Analysis

FE analysis of cone penetration was carried out using ABAQUS, commercially available software (ABAQUS, 2004). The axisymmetric analysis was performed in three stages: pre-processing and post-processing using ABAQUS/CAE, and simulation using ABAQUS/Explicit. The ABAQUS/Explicit numerical procedure was valuable for quasi-static dynamic analysis because it could solve contact problems and large deformations such as cone penetration in soils at a reduced computational time. The explicit dynamic procedure in ABAQUS/Explicit was comprised of nodal acceleration computation at the beginning of the next time increment (eq. 7), solving the equations of motion for the body using the explicit central-difference integration rule (eqs. 8 and 9), and elemental computations of the strain and stress levels using kinematics and the constitutive equations ($\sigma_{(t+\Delta t)} = f(\sigma_{(t)}, d\varepsilon)$). The nodal internal force vector ($I_{(t+\Delta t)}$), which was composed of contributions from the individual elements, was then assembled. All the steps were then repeated for the time increment ($t+\Delta t$). The explicit procedure required no iteration and no tangential stiffness:

$$\ddot{u} = M^{-1} \cdot \left(P_{(t)} - I_{(t)}\right) \qquad (7)$$

$$\dot{u}_{(t+\Delta t/2)} = \dot{u}_{(t+\Delta t/2)} + \frac{\left(\Delta t_{t+\Delta t} + \Delta t_t\right)}{2} \ddot{u}_t \qquad (8)$$

$$u_{t+\Delta t} = u_t + \Delta t_{(t+\Delta t)} \dot{u}_{(t+\Delta t/2)} \qquad (9)$$

where M is the diagonal lumped mass matrix, P is the applied load vector, I is the internal force vector, i is the increment number, u is the displacement, and Δt is the time increment.

The explicit central-difference integration operator is conditionally stable when the time increment (Δt) is less than the stable time increment (Δt_{min}). The stable time increment, which is a requirement for bounded explicit solutions, is the minimum time that a pressure wave takes to move across any element in the model and is dependent on the smallest element dimensions, material stiffness, and material density. An auto-global stable time estimation algorithm that has the capability to continuously update the estimate for the maximum frequency of the entire model was used in the analysis. The capability of automatic update of the time increment is important in the cone penetration problem because of the dynamic changes of element dimensions during cone penetration and the stratified material properties of the soil model.

Auto-adaptive meshing with mesh control was utilized to preserve a high-quality mesh of the soil model during cone penetration and to prevent excessive mesh distortion. The adaptive meshing technique assists the time increment estimation and convergence of solutions in dynamic and quasi-static simulations (Susila and Hryciw, 2003). Adaptive meshing in ABAQUS/Explicit involves a two-step process:
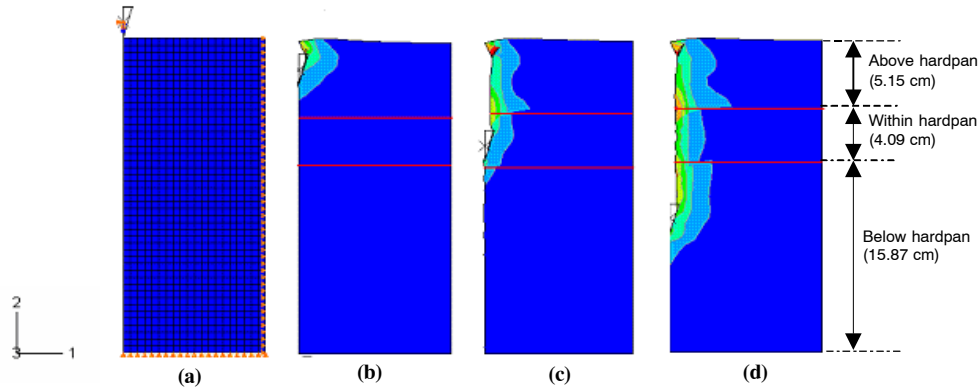
Figure 1. (a) Two-dimensional axisymmetric FE mesh, and plots of the plastic zones when the cone is (b) above the hardpan, (c) within the hardpan, and (d) below the hardpan. The dimensions are shown for compaction II treatment. The arrows in the soil model (a) indicate boundary conditions that constraint the translational degrees of freedom of the right and bottom edges of the soil.

re-discretization (remeshing) of the structure into a smooth new mesh, and remapping the solution from the old mesh to the new one (ABAQUS, 2004).

Geometry and Boundary Conditions

The axisymmetric model was separated into two bodies: a deformable soil, and a rigid cone (fig. 1a). The soil body with a radius of 10.16 cm was partitioned into three layers that had dimensions similar to the soil column study used for FE verification (table 2). Each soil layer had separate material constitutive parameters and a table of hydrostatic yield stress versus volumetric plastic strain depending on soil moisture content and bulk density values. The soil body was meshed using a 4-node bilinear axisymmetric quadrilateral shell element with a reduced integration and hourglass control (CAX4R ABAQUS element). The soil body was seeded with the same edge mesh size, which was smaller (0.8 × cone radius) than the cone radius to meet the master-slave surface contact algorithm and conditional stability of the explicit procedure. The boundaries on the right and bottom edges of the axisymmetric soil model were constrained in the radial (U1) and vertical (U2) translational degrees of freedom, respectively (fig. 1a). The boundary elements on the right edge of the soil model were located at a radial distance that was 16 times the radius of the cone. The factor of 16 was thought to be sufficient to allow the boundary elements to be beyond the plastic deformation. The topsoil surface where the cone penetrates was not constrained.

The ASAE standard cone (apex angle = 30° and base diameter d = 1.28 cm) was defined as a discrete rigid body elastic material (Young's modulus E = 193050 MPa and Poisson's ratio v = 0.3) and modeled by a 2-node linear axisymmetric element (RAX2 ABAQUS element). A reference node was attached at the center of mass of the cone to govern the motion of the cone. Displacement (U2 = −12.0 cm) was prescribed at the reference node to simulate the cone penetration at a rate of 1.65 cm/s.

A similar insertion rate was used to obtain penetration resistance measurements with a cone penetrometer mounted on a Sintech/2G (MTS Systems Corp., Cary, N.C.) machine. For safety reasons, the insertion rate (1.65 cm/s) was kept slightly below the maximum rate of insertion (1.69 cm/s) that was supported by the machine. The shaft of the cone penetrometer was not included in the analysis, assuming that the penetration force from the shaft is small. The cone was constrained to move only in the vertical direction by assigning boundary elements at the reference node of the cone.

Soil-Cone Contact Interface

The soil-cone interaction was simulated by element-based surface-to-surface (master-slave relationship) contact pair interaction with a frictional behavior type. The rigid cone body, which was chosen as a master surface was in contact with the deformable soil, which was selected as a slave surface. As the master surface was moved past the deformable slave surface, the shear and normal forces across this interface were computed. The relative motion of the two surfaces was modeled using a finite sliding formulation that allows arbitrary separation, sliding, and rotation of the surfaces. The kinematic contact algorithm was used for enforcing contact constraints by applying sticking force constraints at the interface between the two surfaces (ABAQUS, 2004). In the kinematic method, ABAQUS/Explicit calculates the value of the sticking force at a node from the mass associated with the node, the distance the node has slipped, and the time increment. ABAQUS/Explicit uses the forces and the total inertial masses (slave and master surface nodes) of the contacting interfaces to calculate an acceleration correction, which is used to obtain a corrected configuration.

Frictional surface interactions of the soil with three cone surface conditions were simulated. The cone surface conditions referred to the type of cone materials used in the

Table 2. Actual measured depths of soil above hardpan, within hardpan, and below hardpan in soil column (all values in cm).

Soil Layers	Compaction I			Compaction II			Compaction III		
	Mean	SD	95% CI	Mean	SD	95% CI	Mean	SD	95% CI
Above hardpan	2.53	0.15	2.46 – 2.60	5.15	0.48	4.92 – 5.36	5.28	0.40	5.08 – 5.48
Within hardpan	5.07	0.34	4.92 – 5.22	4.09	0.28	3.97 – 4.22	3.92	0.22	3.81 – 4.03
Below hardpan	18.67	0.59	18.39 – 18.94	15.87	1.12	15.36 – 16.38	15.19	0.56	14.91 – 15.47

**Table 3. Coefficient of friction for soil and cone materials (Metal, Tmetal, and Teflon)
at two soil moisture contents and two bulk densities of Norfolk sandy loam soil.**

Soil MC (% d.b.)	Dry Bulk Density (Mg m⁻³)	Soil-Material Coefficient of Friction (μ soil-cone surface)[a]					
		Metal		Tmetal		Teflon	
		Mean	SD	Mean	SD	Mean	SD
5	1.22	0.37	0.03	0.27	0.03	0.33	0.01
	1.67	0.51	0.05	0.36	0.01	0.31	0.02
10	1.22	0.49	0.01	0.29	0.03	0.31	0.01
	1.67	0.62	0.01	0.35	0.04	0.30	0.01

[a]   Metal is stainless steel and Tmetal is Teflon-coated stainless steel.

penetration tests for FE model verification. The cone materials were stainless steel (Metal), Teflon-coated stainless steel (Tmetal), and Teflon. The soil-cone coefficient of friction values used in the analysis were obtained from the experiment carried out to determine soil-cone coefficients of friction for the different soil moisture contents, bulk density values, and cone surface conditions (table 3).

FE Outputs

ABAQUS/Explicit outputs for contact interfaces of cone and soil, displacement of the cone, and plastic strain and stress levels of the soil body were obtained. The plastic strain and stress levels were obtained for contour map generation. The resultant forces from contact normal and frictional shear forces associated with the interaction of the cone and soil, and the vertical displacement (U2) of the cone, were obtained to simulate the cone penetration resistance and depth relationships.

EXPERIMENT FOR VERIFICATION OF FE PREDICTION OF HARDPAN LOCATION

A soil cone penetration experiment was conducted to verify the FE model and prediction of hardpan location. Norfolk sandy loam (Typic Paleudults) soil for the experiment was obtained from the soil bin in the NSDL in Auburn, Alabama. The particle size distribution included 72% sand, 17% silt, and 11% clay (Batchelor, 1984). The experiment was carried out using a split-plot design with three replicates. Bulk density (within hardpan) was a main plot treatment with three compaction levels: compaction I, compaction II, and compaction III. Soil moisture was a subplot treatment. Cone surface condition was a sub-subplot treatment. For the bulk density treatment factor, three layers of soil (above, within, and below the hardpan) that varied in bulk density were

created in a graduated plastic cylinder (20 cm dia. × 28 cm height) by applying axial loading using a rigid cylindrical piston.

First, 2 mm sieved soil samples were brought to a soil moisture content of 5% d.b. and kept in tightly closed plastic bags for at least a week to equilibrate the soil moisture. A loose soil sample of predetermined mass was carefully dropped and leveled in the cylinder. A piece of tissue paper with a hole in the center for insertion of the cone penetrometer was laid carefully on the soil. The tissue paper was used to assist in the depth measurement of the soil layers after compression. The soil sample was compressed to a target sample height to obtain the bulk density of the soil below the hardpan.

Next, soil layers within the hardpan and above the hardpan were similarly prepared to obtain the bulk density treatments of the respective soil layers. The bulk density values for each layers are shown in Table 4. The soil column samples were then wetted to near saturation and put in a greenhouse at the NSDL until the soil moisture suction measured using tensiometers inserted at the hardpan depth reached 10 kPa (soil moisture level I) or 60 kPa (soil moisture level II). Once the soil samples of each bulk density treatment reached the desired soil moisture levels (table 5), single-probe cone penetrometer data were collected in each cylinder at 25 Hz using a randomly selected cone material (Metal, Tmetal, or Teflon). The dimensions of the cone (30° circular cone and 12.83 mm cone base diameter) and the probe (9.53 mm shaft diameter) were defined according to the ASAE standard soil cone penetrometer specifications (*ASAE Standards*, 1999a).

A separate experiment was conducted with three replicates to determine the soil-cone (Metal, Tmetal, and Teflon) coefficients of friction according to the Coulomb friction criterion. Soil samples (2 mm sieved) equilibrated to 5% and

**Table 4. Dry bulk density from the laboratory experiment of soil layers (above, within, and below
the hardpan) for three compaction levels of Norfolk sandy loam soil (all values in Mg m⁻³).**

Soil Layers	Compaction I			Compaction II			Compaction III		
	Mean	SD	95% CI	Mean	SD	95% CI	Mean	SD	95% CI
Above hardpan	1.32	0.08	1.28 – 1.36	1.27	0.09	1.22 – 1.31	1.27	0.08	1.23 – 1.31
Within hardpan	1.32	0.09	1.28 – 1.36	1.64	0.11	1.59 – 1.68	1.71	0.09	1.66 – 1.75
Below hardpan	1.25	0.04	1.23 – 1.27	1.48	0.06	1.46 – 1.51	1.54	0.06	1.51 – 1.57

**Table 5. Soil moisture content at three positions (above, within, and below the hardpan) for the two
soil moisture levels and three compaction levels of Norfolk sandy loam soil (all values in % d.b.).**

Soil Layers	Soil Moisture Level I (8.78% d.b.)						Soil Moisture Level II (4.17% d.b.)					
	Compaction I		Compaction II		Compaction III		Compaction I		Compaction II		Compaction III	
	Mean	SD	Mean	SD	Mean	SD	Mean	SD	Mean	SD	Mean	SD
Above hardpan	6.20	1.94	6.08	1.95	7.72	1.38	2.47	0.30	3.02	0.32	2.40	0.15
Within hardpan	8.08	1.53	8.08	2.22	9.25	1.40	4.41	0.55	4.97	0.21	3.83	0.23
Below hardpan	10.26	3.08	9.53	3.25	10.31	1.99	5.05	0.79	5.43	0.26	4.21	0.26

10% (d.b.) moisture contents were placed in a wooden box. For each soil moisture content, the soil was compressed to two bulk densities (1.22 and 1.67 Mg m^{-3}). Bars (0.6 cm thickness, 15 cm length, and 15 cm width) made of stainless steel, Teflon, and Teflon-coated steel were prepared. For the Teflon-coated stainless steel, dry powder Teflon (fluorotelemeter powder) was sprayed on a stainless steel piece and dried before taking measurements. The bars were laid on top of the soil. The pull force required to slide the bar over the soil with normal weights of 2, 11, and 22 kg on top of the bar was measured using a load cell. The coefficients of soil-material friction were determined by estimating the slope of a line fitted to the normal force and average sliding force relationship.

DATA ANALYSIS

Treatment effects of soil moisture, bulk density, and cone surface on prediction of the hardpan location and on penetration resistance were analyzed using appropriate statistical procedures in SAS (2001). Similarly, FE predictions of the hardpan were compared with those obtained experimentally. An F-test statistic with an alpha (α) level of 0.05 was used for all treatment and method comparisons.

RESULTS AND DISCUSSION

The values of the bulk density within the hardpan as shown in table 4 represented the three compaction treatments (compaction I, compaction II and compaction III). The bulk density levels in the compaction II and compaction III treatments (table 4) were significantly greater than the bulk density levels in soil above and below the hardpan (P < 0.0001). To investigate the effects of soil parameters on FE prediction, statistical analyses were performed for only the compaction II (1.64 Mg m^{-3}, soil within hardpan) and compaction III (1.71 Mg m^{-3}, soil within hardpan) because no statistical variations in bulk density values were observed among the soil layers for compaction I. A linear relationship was observed between the predicted bulk density from equation 5 and the observed bulk density from the triaxial stress test with a high correlation coefficient (r^2 = 0.96) and 95% confidence intervals of [−0.14, 0.02] and [0.97, 1.07] for the intercept and slope, respectively. For the FE analysis, the bulk density values (table 4) that were obtained in the soil

column study were used for the bulk density (ρ_ξ) in equation 6 to determine the natural volumetric strains.

The stress-strain relationships for the three layers of the three compaction treatments are shown in figure 2. The differences in bulk density values were manifested in the stress-strain relationships. The natural volumetric strains for the within-hardpan layer were smaller than the above- and below-hardpan layers (fig. 2b and 2c). Tangential Young's modulus values were estimated from each of the curves in figure 2. The mean value of the tangential Young's modulus for each soil layer was estimated for use in the FE analysis.

HARDPAN LOCATION PREDICTION USING CONE PENETROMETER AND FINITE ELEMENT

The predicted results showed considerable oscillation, which is typical in simulating contact problems and may be attributed to the auto-global stable time estimation algorithm in ABAQUS/ Explicit. A moving average filtering technique was performed on the FE data to remove this noise. Following the smoothing treatment, the experimental and predicted penetration resistance plotted as a function of depth exhibited similar trends (figs. 3 and 4). The FE results showed two deflection points (an example is shown in fig. 4c): one near the start of the hardpan (1), and another near the peak cone penetration resistance (2). The penetration resistance obtained with the FE analysis overestimated the experimentally measured cone penetration resistance (fig. 3) for soil moisture level I (8.78% d.b.). The FE model better approximated the experimentally measured penetration resistance profile in the dry soil condition (soil moisture level II, 4.17% d.b.) than in the wet soil condition, except at the high measured cone penetration resistance (fig. 4c). The differences in the FE and cone penetrometer results could possibly be due to the fact that the FE model may not account for all soil failure modes (shear, tensile, and cutting) that occurred during cone penetration because the soil constitutive model used in the analysis incorporated only the hydrostatic compaction behavior. A constant Poisson's ratio assumption may be another possible reason for the differences. Prediction might be improved if the variable tangential Poisson's ratio were used in the analysis, as proposed by Raper and Erbach (1990). They reported that increasing the Poisson's ratio could increase the vertical stress and decrease the strain levels in the soil.
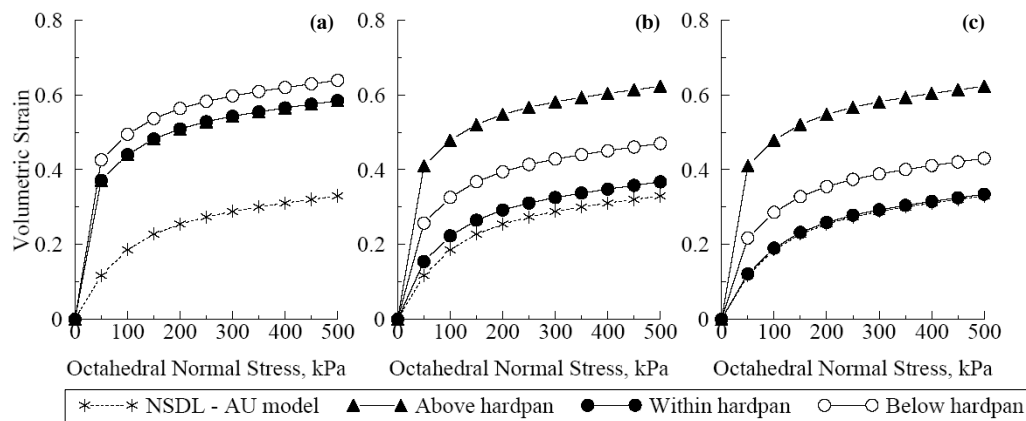
Figure 2. Natural volumetric strains versus octahedral stress for (a) compaction I (1.32 Mg m^{-3} within hardpan), (b) compaction II (1.64 Mg m^{-3} within hardpan), and (c) compaction III (1.71 Mg m^{-3} within hardpan) and the three soil layers (above, within, and below hardpan).
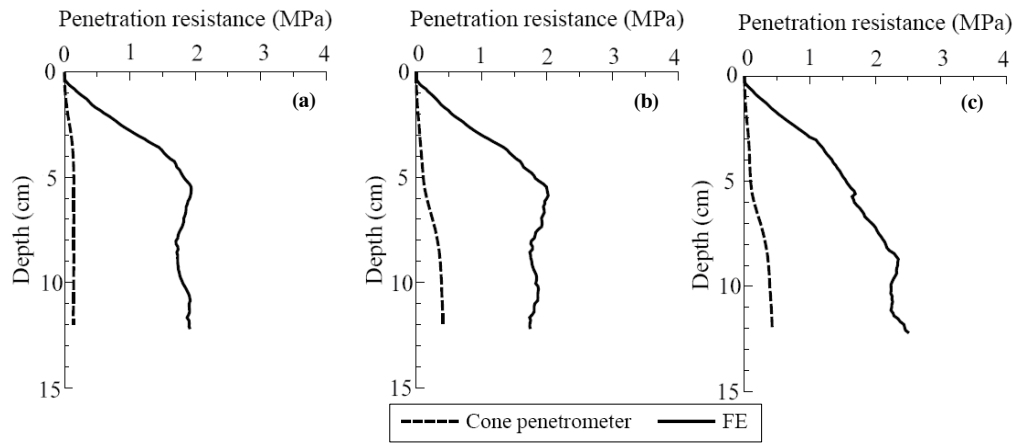
Figure 3. FE predicted and cone penetrometer measured penetration resistance for soil moisture level I (wet; 8.78 % d.b.) at (a) compaction I (1.32 Mg m^{-3} within hardpan), (b) compaction II (1.64 Mg m^{-3} within hardpan), and (c) compaction III (1.71 Mg m^{-3} within hardpan).
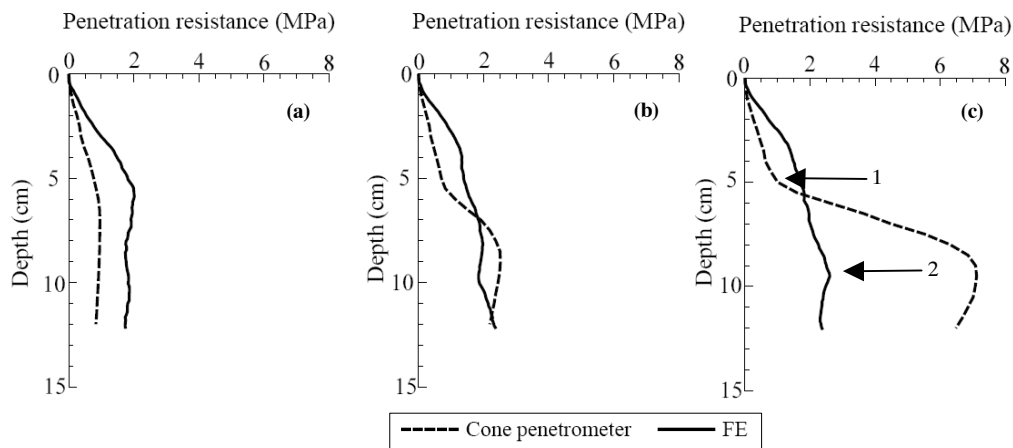
Figure 4. FE predicted and cone penetrometer measured penetration resistance for soil moisture level I (dry; 4.17 % d.b.) at (a) compaction I (1.32 Mg m^{-3} within hardpan), (b) compaction II (1.64 Mg m^{-3} within hardpan), and (c) compaction III (1.71 Mg m^{-3} within hardpan). In the FE results, two deflection points (1 and 2) were observed at locations close to the start of the hardpan and peak penetration resistance.

The hardpan was considered to be located at the depth to the peak penetration resistance of the cone penetrometer data. The hardpan locations from the cone penetrometer measurement and predicted by the FE method were statistically compared. The FE-predicted hardpan depth (7.29 cm) was smaller than cone penetrometer method (11.03 cm) (P < 0.0001). The peak penetration resistance of the cone penetrometer data occurred at the soil below the hardpan, whereas the FE-predicted peak occurred within the hardpan layer (fig. 1 and table 2). The measurement values in table 2 were considered to be the actual depth of the soil layers. The axial loading that was applied to create the hardpan could possibly propagate compression forces to the soil below the hardpan, causing the peak cone penetration resistance from the cone penetrometer to be detected at a deeper soil depth. In the FE model, however, the soil mass elements below the hardpan had the same bulk density values.

The influences of soil moisture content, bulk density, and cone surface on the prediction of hardpan location were analyzed for FE and cone penetrometer methods. The soil moisture content and cone surface strongly affected the cone penetrometer prediction of hardpan depths (P < 0.0001). There were no interaction effects of soil moisture content and cone surface on the predicted depths (P = 0.14). The hardpan depth was not affected by bulk density (P = 0.81). The

predicted hardpan depth in the wet soil condition (8.78% d.b.) was 11.01 cm, and in the dry soil condition (4.17% d.b.), the depth was 8.32 cm, suggesting that soil drying caused the hardpan to be detected at a shallower depth (a difference of 2.69 cm). Varying the coefficient of soil-cone friction affected the hardpan depth prediction, with the depth predicted using the Metal cone (7.19 cm) being shallower than that of the Tmetal (9.96 cm) and Teflon (11.86 cm) cones. When a Teflon cone was used, the predicted depth increased by 65% as compared to the ASAE-standard stainless steel (Metal) cone.

The FE-predicted hardpan locations (table 6) were not significantly affected by the soil moisture (P = 0.73), bulk density (P = 0.48), or cone surface condition (P = 0.59). In the FE model, the hardpan location was predicted at a depth of 7.97 cm in the dry soil and 8.37 cm in wet soil. The FE-predicted hardpan locations by the cone surface conditions were 8.98 cm (Metal), 8.04 cm (Teflon), and 7.50 cm (Tmetal).

Figure 5 shows the influence of cone surface conditions on the penetration resistance profile from cone penetrometer experiments and the FE model. When the Metal cone penetrometer was used, especially in the dry soil conditions (fig. 5b), the highest penetration resistance values were observed, followed by Tmetal and Teflon. The FE model-

Table 6. Cone penetrometer and FE-predicted hardpan depth (all values in cm).

		Cone Penetrometer						FE		
		Metal		Tmetal		Teflon		Metal	Tmetal	Teflon
		Mean	SD	Mean	SD	Mean	SD	Mean	Mean	Mean
Soil moisture level I	Compaction I	6.32	2.42	12.64	1.76	13.74	0.72	4.66	5.87	5.87
(8.78% d.b.)	Compaction II	9.06	1.37	10.31	1.39	13.42	0.72	8.84	6.55	7.90
	Compaction III	7.06	2.61	11.99	2.71	14.26	0.10	9.52	8.85	8.58
Soil moisture level II	Compaction I	11.63	1.91	9.72	0.89	8.88	0.15	5.87	5.47	5.47
(4.17% d.b.)	Compaction II	6.36	0.04	8.54	0.23	10.01	0.63	8.17	8.03	6.95
	Compaction III	6.28	1.41	8.99	0.35	9.75	0.67	9.38	6.55	8.71
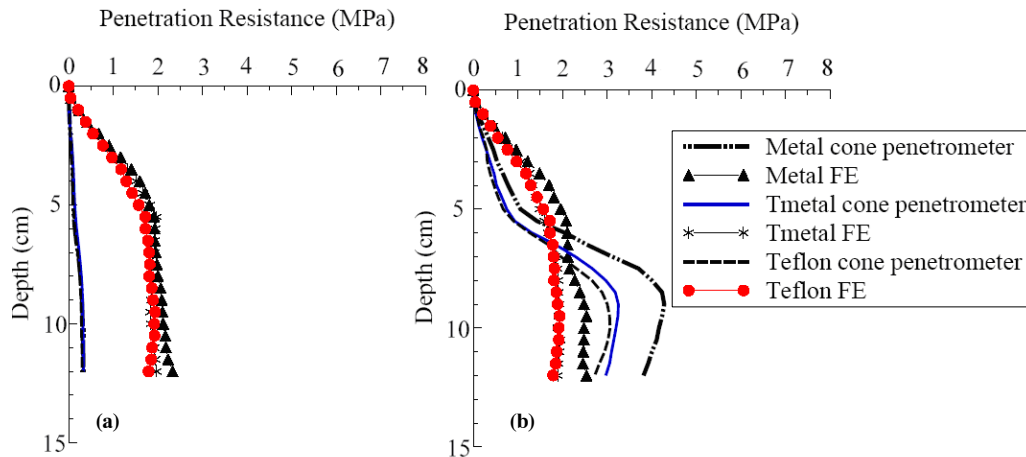
Figure 5. FE predicted and cone penetrometer measured penetration resistance from Metal, Tmetal, and Teflon cone materials for (a) soil moisture level I and (b) soil moisture level II.

simulated penetration resistance profile also showed higher values when the soil-cone coefficient of friction for Metal was used in the analysis. The effects of cone surface on penetration resistance were more distinct in dry than in wet soil conditions.

STRESS AND SOIL DEFORMATION PATTERNS

Penetration of the cone into the soil involves plastic deformations in the vertical and radial directions (figs. 1b, 1c, and 1d). The plastic deformation zone varied by the strength of the soil layers, with the largest and the smallest zones being observed in the soil above and within the hardpan, respectively. Within each soil layer, the shape of the penetration process resembles logarithmic spiral cavity expansion. The plastic deformation that extended from the cone may suggest that the cone penetration resistance was a measure of soil reaction within the zone of influence. Note also that the elements on the soil surface rose up (figs. 1b, 1c, and 1d) as the cone advanced into the soil, which was similar to the penetration behavior observed in the soil column study. The soil deformation patterns also varied due to the effect of soil-cone friction, in that the plastic strain levels for Metal were higher than for Teflon and Tmetal (figure not shown).

The FE model provided good insight into understanding the soil mechanical behavior during cone penetration for different soil-cone contact (friction) surfaces in stratified soil layers with varying soil conditions. Determination of soil strength and location of compacted layers (hardpans) are important applications of the cone penetration method. In this study, the FE method better approximated the penetration resistance profile for predicting hardpan location than did the magnitude of the penetration resistance. Due to the limitations of the FE method,

soil material behavior (shear and cutting) may not be approximated well enough for modeling material discontinuity and soil constitutive relationships.

The FE modeling of cone penetration could be further improved in future studies, in particular for predicting the magnitude of penetration resistance, by including the pre-consolidation stress concept in the soil constitutive model, the flow rule defined based on non-associative plasticity, and variable linear elastic parameters (Young's modulus E, and Poisson's ratio ν). Future FE analysis of cone penetration in layered soil that varies in soil types (e.g., clay and sand soil interfaces) is also important to simulate penetration resistance in the stratified soil profiles found in many crop fields.

CONCLUSIONS

From the finite element analysis of cone penetration on Norfolk sandy loam soil for predicting hardpan depth, the following conclusions were drawn:

- The finite element model developed in ABAQUS was able to simulate cone penetration in a layered Norfolk sandy loam soil that varied in soil moisture content and bulk density.
- The FE model predicted the hardpan location at depths shallower that the depths measured by the cone penetrometer method.
- Soil moisture significantly affected the hardpan location as determined from the cone penetrometer data (P < 0.0001). The FE-predicted hardpan location did not vary with soil moisture (P = 0.73).

REFERENCES

ABAQUS. 2004. *ABAQUS Version 6.4.* Providence, R.I.: ABAQUS, Inc.

ASAE Standards. 1999a. S313.3: Soil cone penetrometer. St. Joseph, Mich.: ASAE.

ASAE Standards. 1999b. EP542: Procedures for using and reporting data obtained with the soil cone penetrometer. St. Joseph, Mich.: ASAE.

Bailey, A. C. 2004. Unpublished data. Auburn, Ala.: USDA-ARS National Soil Dynamics Laboratory.

Bailey, A. C., and C. E. Johnson. 1989. A soil compaction model for cylindrical stress states. *Trans. ASAE* 32(3): 822-825.

Bailey, A. C., and C. E. Johnson. 1994. NSDL-AU model, soil stress-strain behavior. ASAE Paper No. 941074. St. Joseph, Mich.: ASAE.

Bailey, A. C., and C. E. Johnson. 1996. Soil critical state behavior and the NSDL-AU model. ASAE Paper No. 961064. St. Joseph, Mich.: ASAE.

Batchelor, J. A. 1984. Properties of bin soils. Auburn, Ala.: USDA-ARS National Tillage Machinery Laboratory.

Chen, W. F., and E. Mizuno. 1990. *Non-Linear Analysis in Soil Mechanics: Theory and Implementation*. Developments in Geotechnical Engineering, Vol. 53. Amsterdam, The Netherlands: Elsevier.

Chiroux, R. C., W. A. Foster Jr., C. E. Johnson, S. A. Shoop, and R. L. Raper. 2005. Three-dimensional finite element analysis of soil interaction with rigid wheel. *Applied Math. and Computation* 162(2): 707-722.

Farrell, D. A., and E. L. Greacen. 1966. Resistance to penetration on fine probes in compressible soil. *Australian J. Soil Res.* 4: 1-17.

Foster, Jr. W. A., C. E. Johnson, R. C. Chiroux, and T. R. Way. 2005. Finite element simulation of cone penetration. *Applied Math. and Computation* 162(2): 735-749.

Gill, W. R. 1968. Influence of compaction hardening of soil on penetration resistance. *Trans. ASAE* 11(6): 741-745.

Gill, W. R., and G. E. VandenBerg. 1968. *Soil Dynamics in Tillage and Traction.* Agriculture Handbook No. 316. Washington. D.C.: USDA.

Grisso, R. D. 1985. Compaction of agricultural soil by continuous deviatoric stress. PhD diss. Auburn, Ala.: Auburn University, Department of Agricultural Engineering.

Lunne, T., P. K. Robertson, and J. J. M. Powell. 1997. *Cone Penetration Testing in Geotechnical Practices*. London, U.K.: Blackie Academic and Professional.

Markauskas, D., R. Kacianauskas, and M. Suksta. 2002. Modeling the cone penetration test by the finite element method. *Foundations of Civil and Environ. Eng.* 2: 125-139.

Mouazen, A. M., and H. Ramon. 2002. A numerical-statistical hybrid modeling scheme for evaluation of draught requirements of a subsoiler cutting a sandy loam soil, as affected by moisture content, bulk density, and depth. *Soil Tillage Res.* 63(3-4): 155-165.

Mulqueen, J., J. V. Stafford, and D. W. Tanner. 1977. Evaluation of penetrometers for measuring soil strength. *J. Terramechanics* 14(3): 137-151.

Raper, R. L., and D. C. Erbach. 1990. Effect of variable linear elastic parameters on finite element prediction of soil compaction. *Trans. ASAE* 33(3): 731-736.

Raper, R. L., D. W. Reaves, J. N. Shaw, E. van Santen, and P. L. Mask. 2005. Using site-specific subsoiling to minimize draft and optimize corn yields. *Trans. ASAE* 48(6): 2047-2052.

Rohani, B., and G. Y. Baladi. 1981. Correlation of mobility cone index with fundamental engineering properties of soil. In *Proc. 7th Intl. Conf. of the Intl. Society of Terrain-Vehicle Systems.* 3: 959-990. Calgary, Alberta, Canada.

Sanglerat, G. 1972. *Interpretation of Penetration Diagrams: Theory and Practice.* Developments in Geotechnical Engineering. Amsterdam, The Netherlands: Elsevier.

SAS. 2001. *SAS Version 8.02.* Cary, N.C.: SAS Institute, Inc.

Susila, E., and R. D. Hryciw. 2003. Large displacement FEM modeling of the cone penetration test (CPT) in normally consolidated soil. *Intl. J. Numer. Anal. Methods* 27(7): 585-602.

Tollner E. W., B. P. Verma, and J. M. Cheshire. 1987. Observing soil-tool interactions and soil organics using X-ray computer tomography. *Trans. ASAE* 30(6): 1605-1610.

Upadhyaya, S. K., U. A. Rosa, and D. Wulfsohn. 2002. Chapter 2: Application of the finite element method in agricultural soil mechanics. In *Advances in Soil Dynamics*, 2: 117-1153. S. K. Upadhyaya et al., ed. St. Joseph, Mich.: ASAE.

Yu, H. S., and J. K. Mitchel. 1998. Analysis of cone resistance: Review of methods. *J. Geotech. and Geoenviron. Eng.* 124(2): 140-149.